Modelling and optimisation of acoustic inertance segments for thermoacoustic devices

Luke Zoontjens, Luke, Carl Q. Howard, Carl, Anthony C. Zander, Ben S. Cazzolato, B

School of Mechanical Engineering, The University of Adelaide, Australia

ABSTRACT

Thermoacoustic devices may use high-amplitude sound waves to serve a variety of purposes such as cryogenics, domestic refrigeration, electricity generation or warning siren systems. In all designs, there is a transfer of acoustic power between the various 'sources' and 'sinks', especially at very high acoustic pressure levels (170dB+) and velocity amplitudes (which are significant fractions of the local Mach number). Inertance segments, in which the oscillatory flow is accelerated, represent a design challenge in balancing frictional or viscous losses with improvements to the compactness, weight and performance of the overall system. This paper considers optimisation of an inertance segment used in a standing-wave type heat-driven thermoacoustic device and compares experimental data with results obtained from numerical finite element modelling, acoustic transmission line theory and linear thermoacoustic formulations.

INTRODUCTION

Ideally, proponents of alternative energy technologies to those used in the Australian energy industry should be at least aware of the benefits and drawbacks of thermoacoustics. Thermoacoustic devices may use high-amplitude sound waves to serve a variety of purposes such as cryogenics, cost-effective domestic refrigeration, electricity generation or warning siren systems, without drawbacks such as expensive construction or maintenance costs, high part counts or adverse environmental impact.

The principle of operation of a thermoacoustic device could be explained as 'exploiting' the temperature changes of a volume of gas as its pressure oscillates. These temperature changes are so small at audible sound levels that they are considered trivial for consideration of issues such as environmental noise or optimisation of acoustic performing spaces. As Garrett and Backhaus (2000) note, even at sound levels considered painful to the human ear – around 120dB re 20μPa – these temperature changes are small, of the order of hundredths of a degree Celsius. But within thermoacoustic devices in which the pressure amplitude levels are in excess of 170dB and often higher than 190dB, the temperature changes are of such magnitude that effective heat exchanges occur.

Further to previous work (Zoontjens et al. 2005b) in the development of thermoacoustics for automotive air-conditioning systems, a thermoacoustic refrigerator which operates using a heat source has been developed at The University of Adelaide. A model of this device, termed the Heat Driven Thermoacoustic Refrigerator or 'HDTAR', is shown in Figure 1.

As shown in Figure 1, the HDTAR is here considered as comprising three components: a thermoacoustic engine which uses a temperature differential to generate acoustic work (the acoustic 'source'), a thermoacoustic heat pump which uses acoustic work to generate a temperature differential (the acoustic 'sink') and a constrictive duct which the heat engine and heat pump are attached to each end. The form of the HDTAR is a straight line duct with terminations at each end, so a standing wave (with volume velocities greatest in the midcentre) will develop during operation. The constrictive duct is termed an inertance, the acoustical equivalent to the AC electrical term 'inductance', since the narrow constriction forces the oscillating gas to accelerate through to the other end. This constriction reduces the system size and weight whilst maintaining preferable operating frequencies. Further to previous studies of acoustic inertance losses, this investigation will consider the thermoacoustic power output and efficiency in the optimisation of the inertance section.

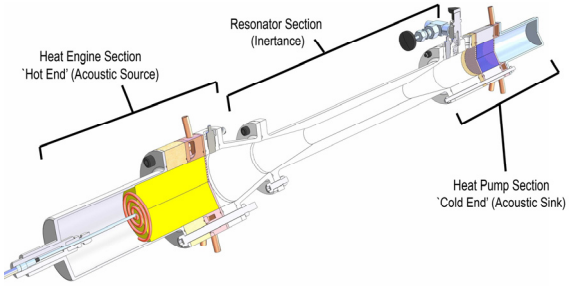

Figure 1. Computer model showing a sectional view of the Heat Driven Thermoacoustic Refrigerator (HDTAR) under development

However, the narrow section of the inertance led to concerns regarding viscous or dissipative losses in the transmission of acoustic power between the heat engine and the heat pump. These concerns therefore motivated a study in the design phase of the device using numerical methods available such as *DeltaE* (Ward & Swift 2001). The study was designed to show the influence of throat radius and the dynamic viscosity (and hence viscous losses) of the working fluid upon the closed form (pressurised) HDTAR engine. The addition of the heat pump section was not considered necessary for the study of the inertance losses and on this basis has been omitted.

This paper will first demonstrate the usage and effectiveness of *DeltaE* for the design of practical thermoacoustic devices. Next, this paper will present the modelling techniques and results for the design of the inertance section of the HDTAR. The effect of viscous and frictional losses in the inertance section are modelled using *DeltaE* and also *ANSYS*. Finally,

this paper will compare experimental results obtained from the HDTAR using the manufactured inertance section.

DELTAE

The first-order linear thermoacoustic approximations developed by Rott (1980) perhaps comprised the first quantitative representation of thermoacoustic devices. With sufficient boundary condition data, Rott's acoustic approximations could be used to estimate the steady-state complex pressure, complex volume velocity and temperature of the working gas in one-dimension along the centre axis of the device.

Specifically, these two approximations were summarised by Swift (2002, Equations 4.54, 4.70) and are reproduced in Equations 1 and 2. Based upon conservation of momentum and continuity, these two expressions relate the complex pressure and velocity with one-dimensional temperature gradients in the thermoacoustic channel. Using a suitable discretisation method for the axial direction x, this enables resolution of the complex pressure dp_1, complex volume velocity dU_1 and temperature T at all positions within the device. This is a basic description of the method implemented in the thermoacoustic modelling program *DeltaE* (Ward & Swift 2001). The Design Environment for Low-Amplitude Thermoacoustic Engines (*DeltaE*) was developed by researchers in thermoacoustics in the United States (Ward & Swift 2001). Although it seems it was primarily intended for the design of thermoacoustic systems, and as such is not widely used amongst acousticians in Australia, this program is actually a very effective tool for any one-dimensional internal acoustic network, such as plane-wave propagation in pipe or duct systems.

$$dp_1 = -\frac{j\omega\rho_m dx/A}{1-f_\upsilon}U_1 \tag{1}$$

$$dU_1 = -\frac{j\omega A dx}{\gamma p_m}\left[1+(\gamma-1)f_\kappa\right]p_1 + \frac{(f_\kappa - f_\upsilon)}{(1-f_\upsilon)(1-\sigma)}\frac{dT_m}{T_m}U_1 \tag{2}$$

DeltaE is effective for the initial design of low-amplitude thermoacoustic systems, whereby the flow is considered laminar, and higher-order effects (such as entropy generation, turbulence, and Rayleigh streaming) are considered to be of little importance. However, a purposeful thermoacoustic refrigerator is likely to use high-amplitude sound waves, or a drive ratio (ratio of dynamic pressure amplitude $|p_1|$ to mean pressure p_m) in excess of 3%, where non-linear, higher order effects are expected.

In *DeltaE*, the entire system of interest is assembled in segments, such as straight pipes, conical sections, lumped-element volumes and tee-branch connectors. The segments are arranged to form a one-dimensional paths of acoustic propagation. Paths can be looped to form travelling wave devices, non-zero mean fluid flows can be modelled, and all thermophysical properties of the internal fluid and surrounding solid are accessible and adjustable.

DESIGN AIMS AND METHOD

The intent of the study was to optimise the internal geometry of the HDTAR inertance section with acoustic power transmission capacity to be used for a cost function. With the decision to reuse a heat pump section from a previous device (Zoontjens et al. 2005a), the inertance section could be developed without constantly returning to optimise the heat pump section, provided that the thermal and viscous penetration depths (δ_κ and δ_υ respectively) were maintained within predefined tolerances.

As seen in Equations 3 and 4, with wavenumber k, gas density ρ, thermal capacity c_p, and dynamic viscosity μ constant from a design viewpoint, the two parameters δ_κ and δ_υ are most susceptible via the operating frequency ω to the geometry of the inertance and so limits were applied to the predicted operating frequency. For the existing heat pump section to be effective, the operating frequency of the system using helium should be between 305Hz and 365Hz, or for air, approximately 100Hz to 125Hz. A design goal for the inertance section was to achieve an operating frequency in this range.

$$\delta_\kappa = \sqrt{\frac{2k}{\rho c_p \omega}} \tag{3}$$

$$\delta_\upsilon = \sqrt{\frac{2\mu}{\rho\omega}} \tag{4}$$

Without considering the heat pump section, a schematic of the HDTAR in a heat-engine configuration only is shown in Figure 2, with its corresponding *DeltaE* representation in Figure 3.

Figure 2 shows operating parameters of interest for the HDTAR operating as an engine only (i.e. internal heat pump elements omitted). The engine power $\dot{E}_{2,0}$ is defined by Swift (2002) as 2nd order acoustic power leaving the ambient end of the thermoacoustic stack. For experimental studies, the acoustic pressure inside the HDTAR can be evaluated at distances of 0.255m, 0.789m and 0.844m from the 'Hot End' inside wall of the device (where the axial co-ordinate x=0). In varying the throat diameter of the Resonator Section, *DeltaE* was used to predict the operating frequency, acoustic power developed and the engine efficiency η_{engine}. Measuring the heat delivered to the engine $\dot{Q}_{HHX}$ directly is possible but in its current form of construction, the HDTAR will have significant radiant heat flux $\dot{q}_{rad}$ which will lead to inaccurate estimation of $\dot{E}_{2,0}$ and hence η_{engine}.

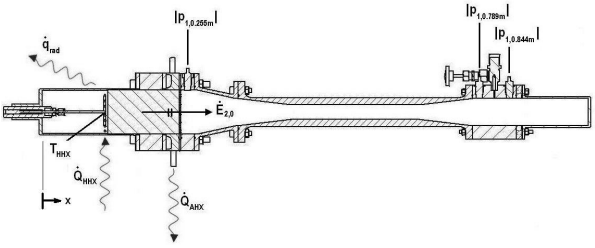

Figure 2. Schematic of the heat-engine only configuration of the HDTAR

Acoustic power produced in the 'hot end' (leftmost ends of Figure 1 and Figure 2) of the device is transferred via the central inertance to the opposing volume. The presence of large acoustic compliances in each end, coupled to a central inertance, is a characteristic shared with double Helmholtz resonators. This arrangement is also displayed in Figure 4 using an AC electrical element analogy, in which one might think of the gas particles accelerating through the inertance section with the acoustic source and sink as compliances at each end.

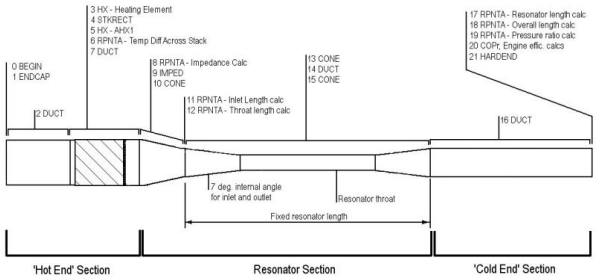

Figure 3. *DeltaE* model sections for heat-driven HDTAR

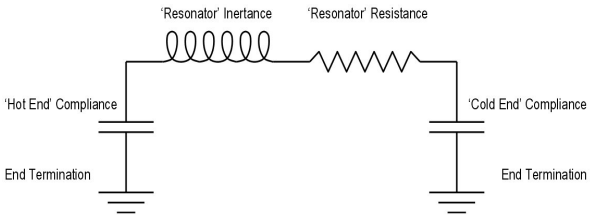

Figure 4. Equivalent 'AC electrical' element diagram of the HDTAR without internal structures

In Figure 4 the viscous losses of the gas flow as it scrubs the inside walls of the resonator are modelled in series (in phase) with the inertance effect, which will of course in turn be 90 degrees out of phase with each compliance element. This resistance component is difficult to model accurately, since the flow is oscillatory and mean and dynamic pressures are high.

As indicated in Figure 3 and Figure 4, the inertance section forms part of the 'Resonator Section' and comprises of a straight circular duct with conical pipe sections used for an inlet and outlet. This section is represented in the *DeltaE* model (Figure 3) as the three segments '13 CONE', '14 DUCT' and '15 CONE'.

By fixing the overall length and inlet angles, increasing the throat diameter in the model would be physically analogous to drilling a larger hole through the resonator throat. As the throat diameter is increased in the model, the lengths of the 'CONE' and 'DUCT' segments must be altered to ensure the internal angle and overall lengths are preserved. This was achieved using mathematical functions embedded into the *DeltaE* model termed "RPNTA" segments. 'RPNTA' segments can be programmed to calculate complex functions at every iteration of the model solution. In this study, two functions were used to calculate the resultant lengths of the 'CONE' and 'DUCT' segments from the throat diameter. The inputs for the length of the segments in the model were set to equal the output of the functions, so whenever the throat radius was changed, the lengths of the 'CONE' and 'DUCT' segments changed accordingly.

DeltaE was programmed to achieve targets for the real and imaginary components of the end impedance and a fixed heat exchanger temperature, by estimating the operating frequency, initial temperature and the acoustic pressure at the hot end of the device, for varying inertance 'throat' radii. An arbitrary heat input of 300W was used to model the operation of the heat engine.

MODELLING RESULTS

DeltaE

The dynamic viscosity of the gas was modelled using a power law approximation to published values of air (Mills 1999) which was then proportionally adjusted for each 'fluid' considered. At standard conditions, atmospheric air has a dynamic viscosity μ of approximately 18.5μkg/ms. Therefore, '10.18 μkg/ms' is effectively atmospheric air modified to possess a dynamic viscosity ~55% of that standard for the temperature range of interest.

Figure 5 shows the relationship between the throat radius of the inertance section and the estimated operating frequency of the HDTAR. Figure 5 indicates that the operating frequency of the engine will increase with increasing throat radius. Increasing the open area of the throat section reduces the inertance effect of the resonator section, shifting the primary mode of oscillation up towards that of a half wavelength standing wave. Indeed, for a throat radius of 0.025m (equal to the radius of the CHX / AHX duct section) and air at an ambient temperature T_m of 300K, the predicted operating frequency of 170.4Hz compares well to the analytical first mode (a simple half-wavelength resonator) at 170.1Hz. Reducing the dynamic viscosity of the gas appears to slightly increase the operating frequency of the device.

A simple estimate of the operating frequency f using a Helmholtz resonator approximation of standard air is provided in Equation 5 (Munjal 1987 Eqn 2.128) where a is the wave speed (here set to 334m/s), S_n is the throat area, l_{eq} is the effective throat length and V_c is the effective compliance.

$$f = \frac{a}{2\pi}\sqrt{\frac{S_n}{l_{eq}V_c}} \tag{5}$$

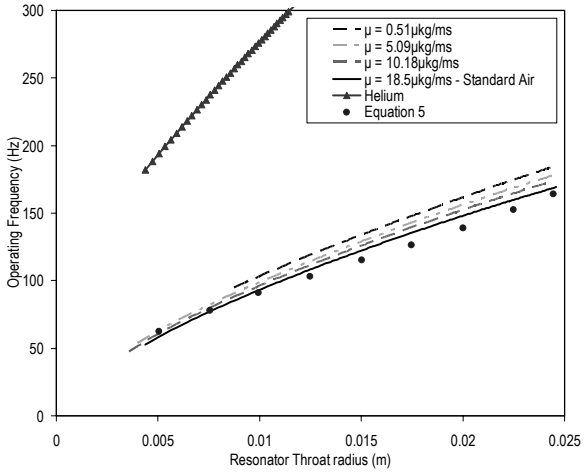

Figure 5. Predicted operating frequency of the HDTAR versus resonator throat radius.

From Figure 5 it can be seen that Equation 5 shows good agreement at small throat radii, where the influence of the inertance section is greatest.

Figure 6 presents the estimated ratio of acoustic pressures (at each end of the resonator section) versus the resonator throat radius. The 'Hot End' (shown in Figure 3) has a cross-sectional area over 2.5 times that of the 'Cold End' in order to amplify pressures in the 'Cold End' section. Figure 6 indicates that there is an optimal resonator throat diameter for maximising this pressure ratio. Although the ratio of cross sectional area between the hot and cold sections is 2.5, note that the pressure ratio between each end is always less than 2.2, and drops to a ratio of ~1.8 for the trivial condition where the throat diameter equals the cold end diameter. This optimum throat diameter is also shown to be dependent on the gas used. For air this maxima is in the range of throat radius around 0.0082m, whereas for helium this maxima is around 0.01m. Using air, the maximum pressure difference of 2.15 corresponds to a sound pressure level increase of 6.6dB

between the two ends of the device for operation using 300W of heat input. The pressure ratio between each end is dependant on the acoustic power produced in the device, since the different geometries at each end leads to differing rates of acoustic losses with increasing pressure and velocity amplitudes.

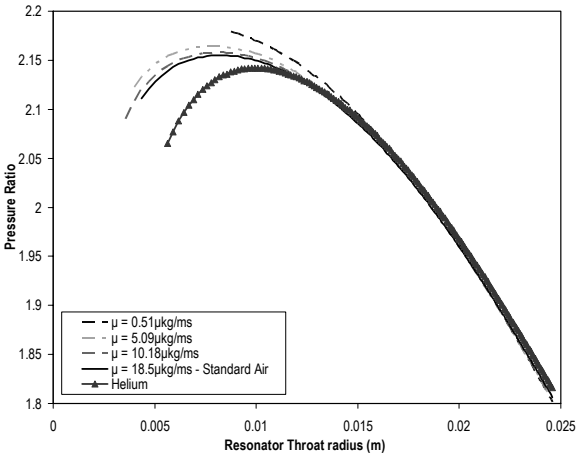

Figure 6. Predicted ratio of acoustic pressures between the inlet and outlet of the resonator versus HDTAR resonator throat radius for the operating mode.

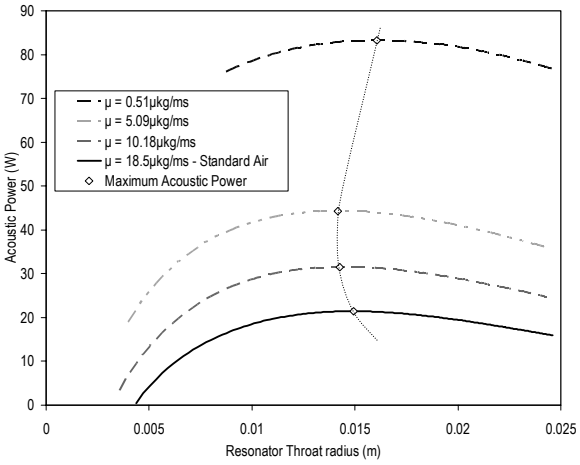

Figure 7. Predicted engine power versus resonator throat radius for the HDTAR.

Figure 7 presents effect of resonator throat radius upon the acoustic power $\dot{E}_{2,0}$ generated by the heat engine. Figure 7 indicates that fluids with lower dynamic viscosities enable increases in the total acoustic engine power created by the stack. Considering that more viscous fluids would suffer greater 'choke' through the inertance, then it follows that the loading faced by the engine stack would be increased. It can be seen from Figure 7 that there is an optimal throat radius for acoustic power output: for air this throat diameter is 0.015m, however for air with lower dynamic viscosity, the throat diameter which yields the greater acoustic outputs is expected to differ. If one considers the inertance section as purely a resistive constriction, then increasing the throat diameter reduces this resistive loss.

The ratio of acoustic power transmitted across the resonator is of significant interest since this will affect the overall efficiency of the thermoacoustic refrigerator. Figure 8 suggests that the acoustic transmissibility is significantly affected by dynamic viscosity; however there is no 'optimal' throat diameter other than increasing the throat area as far as practicable. Fluids with higher dynamic viscosity will incur higher acoustic losses through the inertance, reducing the transmission coefficient. In practice this result is still considered somewhat 'ideal', since entrance and exit losses associated with higher-order flow effects through the conical sections are not accounted for by the model.

The impact of throat diameter upon the engine efficiency is shown graphically in Figure 9. With reference to Figure 8, selection of the throat diameter requires a trade-off between the acoustic power transmitted by the inertance and the efficiency of the engine producing that acoustic power. The instability of the model (caused by excessive velocities) at small throat diameters prevented full generation of plots for fluids with lower dynamic viscosities. In line with Figures Figure 8 and Figure 9, fluids with lower dynamic viscosity enable greater stack efficiencies.

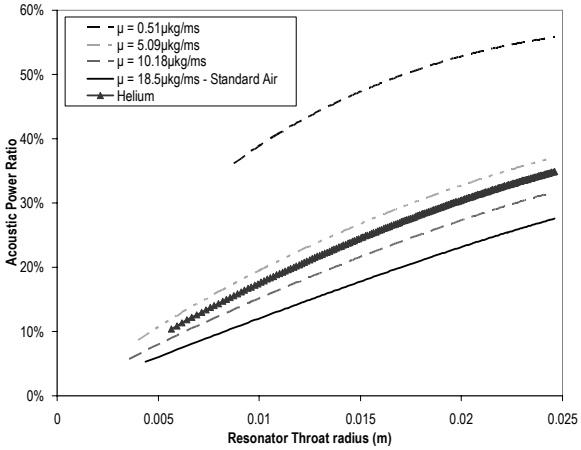

Figure 8. Predicted ratio of acoustic power across the resonator inlet and outlets versus resonator throat radius.

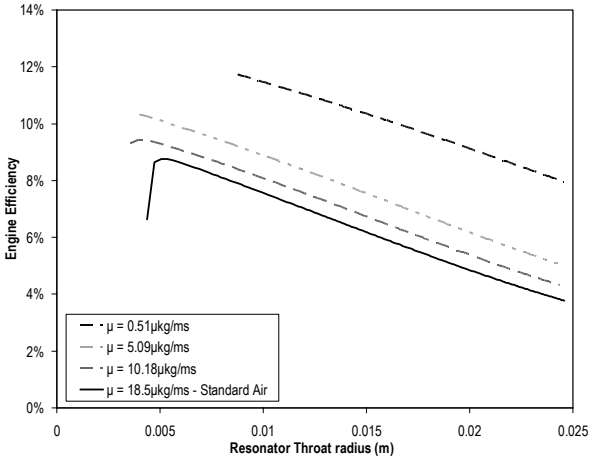

Figure 9. Predicted engine thermal efficiency versus resonator throat radius.

Figure 9 enables some comparison with the expectations of Wetzel & Herman (1997). In the design of thermoacoustic devices, Wetzel & Herman recommend that the Carnot relative coefficient of performance COP_r of a thermoacoustic engine or refrigerator stack be optimised using iterative adjustment of its normalised length ξ and normalised centre position ξ_c as per Equations 7 and 8, where Δx is the stack length, x_c is the stack centre position, a is the wave speed and λ is the wavelength.

$$\zeta = \frac{2\pi\Delta x}{\lambda} = \frac{2\pi f\Delta x}{a} \tag{7}$$

$$\zeta_c = \frac{2\pi}{\lambda} x_c = \frac{2\pi f}{a} x_c \quad (8)$$

With the simulation keeping the length and location of the HDTAR engine stack fixed, ξ and ξ_c are shown by Equations 7 and 8 to be dependant on the operating frequency f. It can be seen that shifts in operating frequency from changes in the inertance of the resonator section will change the operating COP_r of the stack and hence the expected engine efficiency of Figure 9.

Finite Element Modelling

The finite element modelling software called *ANSYS* was used to predict the pressure amplification that occurs with the enclosure described here. Two types of finite elements were used in the modelling, namely elements with only pressure degrees of freedom (called FLUID29 in *ANSYS*), and elements with translational degrees of freedom (FLUID79 in *ANSYS*). The pressure formulated elements in *ANSYS* cannot account for viscous losses at the boundary walls of the enclosure. A novel method of incorporating the effects of viscous losses at the walls was implemented by using displacement formulated elements and attaching viscous dash-pot dampers. Figure 10 and Figure 11 show pictures of finite element mesh of the enclosure using displacement formulated elements.

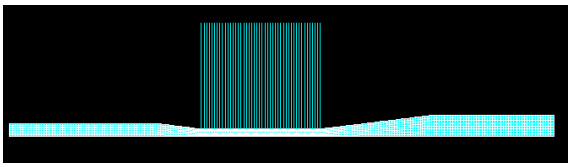

Figure 10. picture of the finite element mesh

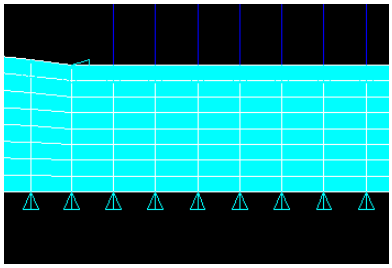

Figure 11. closeup of the mesh.

An equivalent viscous damping coefficient c_v for the losses in wide pipes (Kinsler et al 2000 p230) is

$$c_v = \pi a t \sqrt{2\eta\omega\rho_0} \quad (6)$$

where a is the radius of the pipe, t is the axial length of the element, η is the coefficient of shear viscosity (η=1.85e-5 Pa s for air), ω is the frequency (radians/s), and ρ_0 is the density of air.

Figure 12 shows the predicted resonance frequencies of the enclosure using the pressure and displacement formulated elements. The results show that both methods predicted identical resonance frequencies, as would be expected.

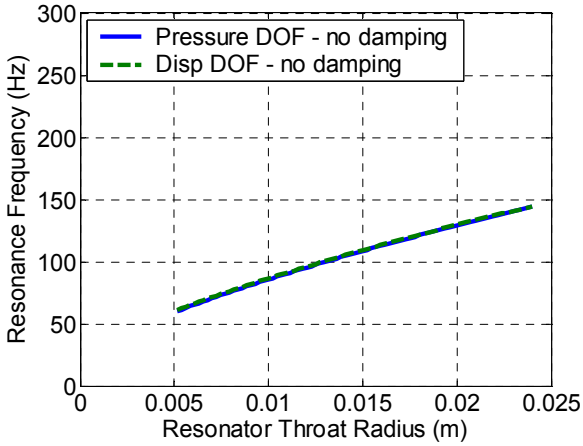

Figure 12. Resonance frequencies of the chamber predicted using pressure and displacement formulated elements (*c.f.* Figure 5).

Figure 13 shows the predicted pressure amplification when using the elements with pressure DOFs with no damping, the displacement formulated elements with no damping, and when using the displacement formulated elements with viscous damping in the restricted section.

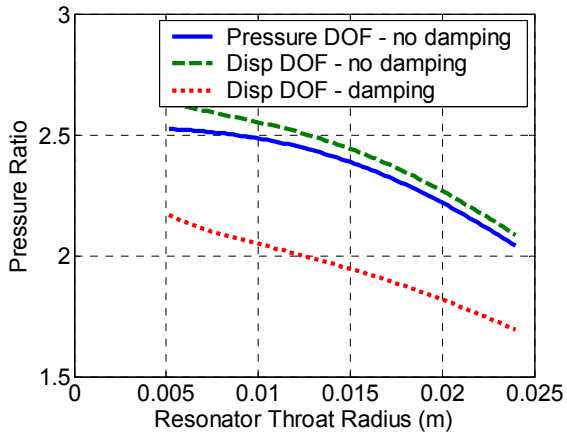

Figure 13. Predicted pressure amplification using a finite element analysis.

Summary of Modelling Outcomes

Both modelling and analytical techniques used suggested that in order to maintain an operating frequency using air of between 100Hz and 125Hz, a throat radius of 0.0112m to 0.015m is required. To maximise the acoustic power produced by the engine, and the transfer of acoustic power across the resonator, the throat radius should be closer to the upper throat radius limit of 0.015m. However to maximise the engine efficiency and the ratio of acoustic pressures, the throat radius should be nearer to the level throat radius limit of 0.0112m.

MANUFACTURING CONSIDERATIONS

Consideration of the manufacture of the resonator section in addition to the estimates of the performance of the device enabled selection of the throat radius. The actual throat diameter was selected to be 0.0271m (radius 0.0135m) based upon consideration of Figure 5 to Figure 9, and the availability of suitable drill pieces. As a machined component from an aluminium billet, the internal pipe walls were sanded smooth, but due to poor access to the interior, could not be polished.

The resultant performance of the HDTAR with respect to the heat applied to the heat engine is expected to be non-linear: Table 1 shows the effect of increasing the heat input applied to the heat engine upon its estimated performance characteristics as considered previously in Figure 5 to Figure 9.

Table 1. Predicted typical operating characteristics for engine-only HDTAR, 1atm air, throat radius 0.0135m, 30W heat input

Parameter	Input power	
	30W	300W
Operating frequency, f	114Hz	114Hz
Sound Press. Level Ampl., $\|p_1\|$*	165dB	186dB
Ratio of $\|p_1\|$ Ampl. (Level)	2.37 (7.5dB)	2.11 (6.5dB)
Acoustic Power, $\dot{E}_{2,0}$	2.4W	21W
Trans. Power Ratio	15%	16%
COP_r	15%	11%
Eng. Thermal Efficiency, η_{engine}	8.5%	6.6%

* re 20μPa

Using this selected throat radius of 0.0135m, Figure 14 shows the *DeltaE* predicted magnitude of pressure and velocity at the first mode operating frequency of 114Hz, with only 3W of heat input. This operating frequency of 114Hz using air at 1 atmosphere is higher than that expected if using a loudspeaker, due to temperature changes in the working fluid in the vicinity of the heat engine.

The standing wave operation of the HDTAR engine is apparent from Figure 14, with a pressure node / velocity antinode inside the resonator. Flow blockages caused by the presence of the heat exchangers and stack (which constitute the heat engine) show as discontinuities in the plot of gas open area.

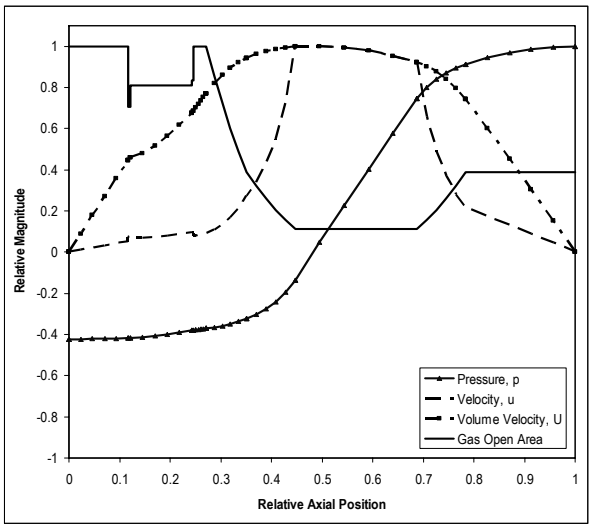

Figure 14. Normalised distribution of predicted state variables for the 'engine-only' configuration of the HDTAR, *f* = 114Hz, 1atm air

Figure 14 and Figure 15 show that there is a sound pressure level 'gain' for the expected operating frequency of the HDTAR. Indeed, the axial area of the 'Cold End' termination is 2.5 times less than that in which the heat engine is located, so in a lossless device a pressure level gain of approximately 8dB is expected between each end. For comparison, the *DeltaE* result shown in Figure 6 expects a pressure level gain of 7.5dB using 3W of heat input (*c.f.* 6.6 with 300W heat input).

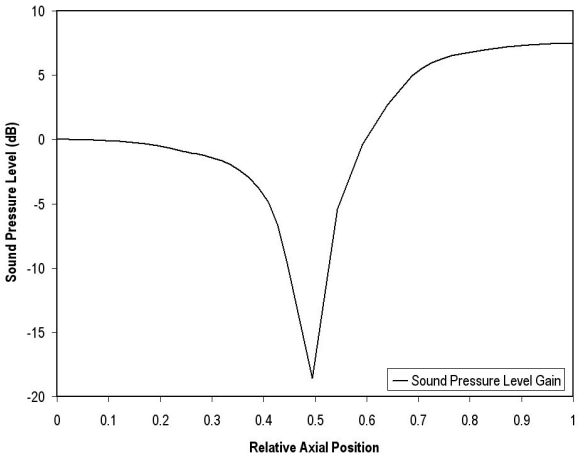

Figure 15. Predicted distribution of sound pressure level normalised to the pressure level at the 'hot' end for the 'engine-only' configuration of the HDTAR, *f* = 114Hz, 1atm air

EXPERIMENTAL VERIFICATION

With the inertance section constructed, a experiment was performed to further demonstrate the capabilities of *DeltaE* for acoustic modelling in pipe networks. With the heat exchangers, stacks and internal blockages removed, a loudspeaker was loosely inserted sideways into the 'hot end' of the empty HDTAR. Using low level random noise, the pressure ratio between pressure transducers mounted at each end of the inertance was experimentally determined. These results were then compared to that expected using *DeltaE*, as shown in Figure 16.

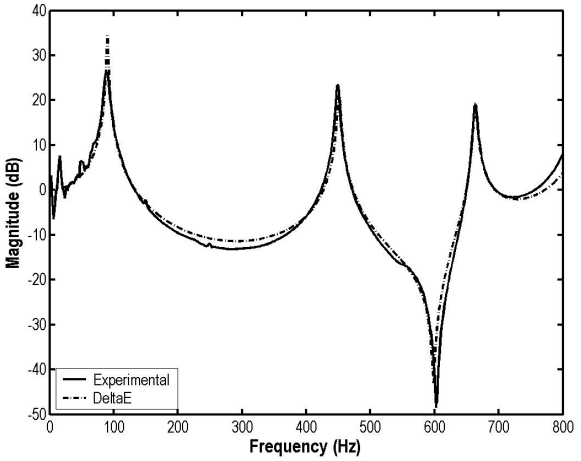

Figure 16. Comparison of experimental results of isothermal pressure ratio with linear-order *DeltaE* predictions

Figure 16 shows good agreement between the experimental and predicted results, with differences in amplitude level for the 2nd and 3rd modes of 2.2dB and 0.5dB respectively, and differences in apparent modal frequency less than 0.5%. At 114Hz, the predicted isothermal pressure ratio level is 6.0dB, compared to 5.3dB experimentally. For this frequency but using a heating element, a pressure ratio level of 7.5dB as shown in Figure 15 is expected by *DeltaE*.

Despite predicting a pressure ratio 6.2dB greater than that measured experimentally, *DeltaE* is still able to provide adequate accuracy to enable design of a device based around this mode of operation.

CONCLUSION

In conclusion, this study has shown that the optimisation of inertance sections cannot be based solely upon acoustic parameters; full consideration must be given to the effect upon the thermoacoustic elements within the acoustic environment such as stacks, regenerators or heat exchangers. Since increasing the throat diameter changes the resistive, inertial and compliant properties of the resonator section, the frequency, pressure and velocity relationships may be altered in nearby stacks or heat exchangers to a point which brings them sub-optimal.

This study gives insight into the highly iterative process of thermoacoustic system design: the vast array of variables which affect the system performance must all be considered as inter-dependent for robust device operation.

REFERENCES

Garrett, S. & Backhaus, S. (2000), *The power of sound*, American Scientist 88(6), 516–525.

Mills, A. (1999), *Heat Transfer*, 2nd Edition, Prentice Hall and NJ and USA.

Munjal, M.L. (1987), Acoustics of ducts and mufflers: with application to exhaust and ventilation system design, John Wiley & Sons, Canada.

Swift, G. (2002), Thermoacoustics: A unifying perspective for some engines and refrigerators, Acoustical Society of America.

Ward, B. & Swift, G. (2001), Design Environment for Low-Amplitude ThermoAcoustic Engines (DeltaE) Tutorial and User's Guide (Version 5.1), Los Alamos National Laboratory.

Wetzel, M. & Herman, C. (1997), *Design optimisation of thermoacoustic refrigerators*, Int. J. Refrig. 20(1), 3–21. Mills 1999.

Zoontjens, L., Howard, C., Zander, A. & Cazzolato, B. (2005a), *Development of a low cost loudspeaker-driven thermoacoustic refrigerator*, Proceedings of Acoustics 2005, Busselton, Western Australia.

Zoontjens, L., Howard, C., Zander, A. & Cazzolato, B. (2005b), *Feasibility study of an automotive thermoacoustic refrigerator*, Proceedings of Acoustics 2005, Busselton, Western Australia.